HHS Public Access

Author manuscript

Neurogastroenterol Motil. Author manuscript; available in PMC 2019 September 01.

Published in final edited form as:

Neurogastroenterol Motil. 2018 September ; 30(9): e13351. doi:10.1111/nmo.13351.

Image velocimetry and spectral analysis enable quantitative characterization of larval zebrafish gut motility

Julia Ganz[*,1,3], **Ryan P. Baker**[*,2], **M. Kristina Hamilton**[1], **Ellie Melancon**[1], **Parham Diba**[1,4], **Judith S. Eisen**[1,+], and **Raghuveer Parthasarathy**[2,+]

[1]Institute of Neuroscience, 1254 University of Oregon, Eugene, OR 97403

[2]Department of Physics, 1274 University of Oregon, Eugene, OR 97403

Abstract

Normal gut function requires rhythmic and coordinated movements that are affected by developmental processes, physical and chemical stimuli, and many debilitating diseases. The imaging and characterization of gut motility, especially regarding periodic, propagative contractions driving material transport, are therefore critical goals. Previous image analysis approaches have successfully extracted properties related to the temporal frequency of motility modes, but robust measures of contraction magnitude, especially from *in vivo* image data, remain challenging to obtain. We developed a new image analysis method based on image velocimetry and spectral analysis that reveals temporal characteristics such as frequency and wave propagation speed, while also providing quantitative measures of the amplitude of gut motion. We validate this approach using several challenges to larval zebrafish, imaged with differential interference contrast microscopy. Both acetylcholine exposure and feeding increase frequency and amplitude of motility. Larvae lacking enteric nervous system gut innervation show the same average motility frequency, but reduced and less variable amplitude compared to wild-types. Our image analysis approach enables insights into gut dynamics in a wide variety of developmental and physiological contexts and can also be extended to analyze other types of cell movements.

Graphical abstract

Abbreviated abstract: We present a new image analysis technique using image velocimetry and spectral analysis that returns quantitative measures of gut contraction strength, frequency, and wave speed that can be used to study gut motility and other cellular movements.

[+]Corresponding authors (JSE, eisen@uoneuro.uoregon.edu; RP, raghu@uoregon.edu).

[3]Current address: Department of Integrative Biology, Michigan State University, 288 Farm Lane, East Lansing, MI 48824

[4]Current address: Department of Pediatrics, Oregon Health & Science University, 3181 SW Sam Jackson Park Rd, Portland, OR 97239

[*]These authors contributed equally

PROFESSOR JULIA GANZ (Orcid ID : 0000-0002-9471-1828)

The authors declare no competing interests.

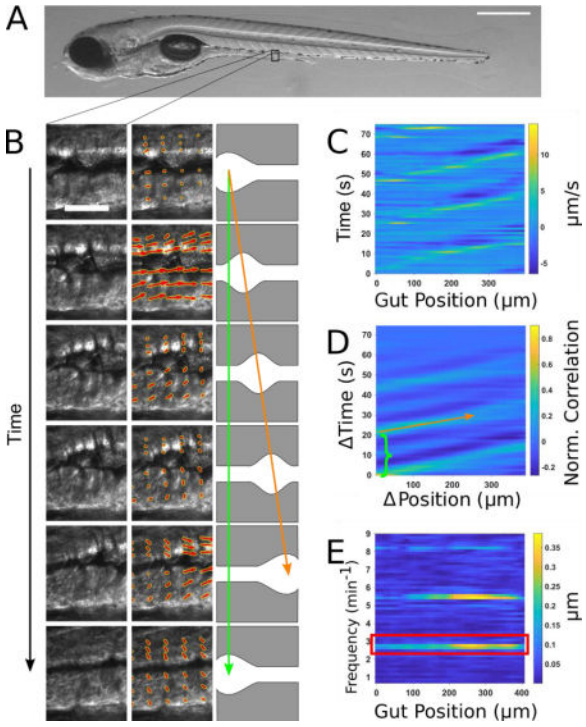

Keywords

intestinal motility; enteric nervous system; Hirschsprung disease

Introduction

Proper gut motility is vital for the health of many organisms, yet measurement and characterization of motility patterns remains challenging, a consequence of both the diversity of gut phenotypes and the limitations of existing analysis and imaging methods. A variety of disorders can alter dynamics of the gut. In humans, for example, inflammatory bowel disease, irritable bowel syndrome, chronic intestinal pseudo-obstruction, Hirschsprung disease, and other ailments typically cause gut dysmotility (1–3). Even within a healthy individual, the gut exhibits different types of movements depending, for example, on its digestive state (4, 5). When fasting, the gut experiences the cyclic sweeping patterns of the migrating motor complex (MMC) (4, 6, 7). The presence of food triggers changes in gut movements that in turn affect the ingested material. Standing contractions serve to mix and break up food, whereas propagating contractions transport contents along the gut (4, 7, 8).

The interplay between the enteric nervous system (ENS) and slow waves generated by the pacemaker-like interstitial cells of Cajal orchestrate gut rhythmic smooth muscle contractions (4, 7, 9). The ENS regulates gut movements through coordinated activation of sensory neurons, as well as both inhibitory and excitatory motor neurons that can be activated by mechanical or chemical stimuli, modified also by gut-extrinsic innervation (4, 7). Although the neuronal circuits and neuronal subtypes that locally regulate contractions have been identified in mammalian models (4, 8), little is known about how these different

neuronal subtypes work together to coordinate and switch between all of the complex motions of the gut. It also remains unclear how gut motility is influenced at the whole organ level by digestive states or other chemical or physiological perturbations (8, 10). Our ignorance stems, in part, from a challenge inherent to the study of gut motility: the gut displays a large variety of dynamic behaviors, yet understanding these behaviors calls for comprehensible characterizations of their parameters.

A common and powerful analysis approach to understanding gut motility involves the generation of spatiotemporal maps (STMaps) from video data (11, 12). To make an STMap, one calculates a one-dimensional measure from each frame of a two-dimensional (2D) video series, for example the luminal diameter at each point along the gut axis or the average image intensity transverse to the gut axis at each point along the gut axis. Plotting this one-dimensional measure for each time-point gives a convenient two-dimensional graph. Correlated patterns, such as traveling waves along the gut, appear as streaks in the plot. A STMap enables straightforward determination of three important parameters of gut motility: the peristaltic frequency, the propagation velocity for peristaltic waves traveling along the gut, and the spatial extent of contractions (11–14). In mammalian systems, STMaps have been generated from videos recorded from dissected guts placed in an organ bath that allow for straightforward edge detection (11, 15) and references therein). Two types of STMaps can be extracted from these video recordings: diameter maps (D-maps) that record diameter changes that relate to circular contractions and, less widely used, longitudinal maps (L-Maps) that record longitudinal contractions (11, 15–21) and references within). D-Maps have been combined with high resolution manometry in which changes in luminal pressure are detected (P-Maps), to determine neuronal activity following gut contraction and relaxation (15, 17, 22).

Despite their utility, there are limitations to existing spatiotemporal mapping approaches. One is that quantitative measures of motions transverse to the gut axis, for example intestinal contractions, have only been possible by detection of the luminal “edge” of the gut as viewed from the side. This works well in dissected gut tissue, because the gut is isolated in a tissue-free environment and so the contrast of the luminal edge is strong, but is very difficult to achieve when imaging inside a living animal, where the contrast between the luminal edge and epithelial cells is weak, even when using high-contrast methods such as differential interference contrast (DIC) microscopy. STMaps that have been generated when imaging a live animal, for example in zebrafish, have relied on using the average image intensity transverse to the gut axis as the mapped feature, which provides only qualitative measures of contraction strength. Another limitation has been the rather small set of parameters extracted from traditional STMaps, expansion of which would allow finer characterization of different physiological states.

In this study, we report a new image analysis technique that returns quantitative measures of gut contraction strength, as well as frequency and wave speed using high-resolution DIC images of sections of the gut imaged in a living animal. This approach, described in more detail below, involves applying well-established image correlation techniques to videos of gut motility, and analyzing the magnitude of dominant periodic modes via Fourier transformation. Notably, previously developed L-Map techniques also make use of image

correlations, assessing the longitudinal displacements of landmarks such as intestinal vasculature (21). By evaluating two-dimensional image correlations we are able to provide equivalent quantitative measures of gut motion across either the longitudinal or transverse gut axis, even in the absence of strong image features, and the isotropy of the analysis allows straightforward comparison of each type of motion.

We apply and assess our new analysis technique using images of guts in living zebrafish larvae, obtained from a custom built differential interference contrast microscope (DICM) (23). Zebrafish are ideally suited for *in vivo* imaging because of their external development and optical clarity during embryonic and larval stage. These features enable measurements of gut motility parameters in intact, living animals, which provides the unique opportunity to combine gut motility parameters with functional analyses in living animals. In addition, zebrafish is an important animal model for studying gut development and function, including aspects of human gut diseases (24–26) and gut microbiota function and dynamics (24, 27, 28). DICM provides high contrast and high resolution optical sectioning, therefore enabling robust image-based calculations. Our method can be more generally used, however, and should, for example, be applicable to dissected preparations commonly used in studies of mammalian guts. Also, as our method is agnostic as to which type of images are analyzed, it can be used for a variety of cellular movements.

To validate our methods, we examine the effects on larval zebrafish gut motility parameters of a chemical stimulus, a physical perturbation, and a biological deficiency, namely acetylcholine, food, and absence of an enteric nervous system, respectively. We find that acetylcholine-treated larvae show a previously reported increase in contraction frequency (14, 29) as well as a newly reported increase in contraction amplitude. Comparing gut motility parameters in fed versus unfed larvae, we find that feeding increases contraction frequency and sustains higher amplitudes over the observed developmental window. Zebrafish larvae lacking ENS innervation show decreased contraction amplitude and also reduced parameter variability compared to wild-type siblings. In addition, imaging over longer intervals reveals highly variable gut motility patterns within individual larvae that appear to be ENS-dependent, as the variability of these patterns is lower in mutants lacking ENS innervation. We suggest that our analysis method opens exciting new avenues for studying gut motility in zebrafish and other systems.

The code we developed for this study is freely available on github: https://github.com/rplab/Ganz-Baker-Image-Velocimetry-Analysis. All data values plotted in Figures 3–5 and Supplementary Figure 1–2 are tabulated in the supplemental text file of comma-separated values “supplemental file 1.”

Results

An image analysis technique based on quantitative spatiotemporal maps and spectral analysis identifies gut motility parameters

To distill complex images of gut motility into concise yet meaningful parameters, we developed a new analysis approach using image velocimetry, “the inference of velocity values from image data”, and spectral analysis (Fig. 1). A typical zebrafish imaged at 6 days

post fertilization (dpf) is shown in Fig. 1A. A full description of the technique can be found in the Materials and Methods section; we provide a summary here. In our experiments, videos of zebrafish gut motility were obtained with DICM (Fig. 1B, left column). A velocity map of the material in each image in the series was determined by digital Particle Image Velocimetry (PIV) (30). We used well-established and freely available PIV code (31) that divided each image into a grid of sub-images; the sub-image pairs in adjacent frames that were maximally correlated with each other revealed the frame-to-frame displacement of material in that region, or equivalently its velocity (Fig. 1B, middle column). Areas outside the gut were discarded from the analysis.

Motion along the anterior-posterior (AP) axis, the dorsal-ventral (DV) axis, or any combination of the two can be assessed from the resulting two-dimensional displacement map. Because we were primarily concerned with motion along the AP axis, and its variation along that axis, we typically considered only the AP components of the resulting two-dimensional displacement map, and further condensed these by averaging along the DV. We thereby obtained for each specimen a one-dimensional curve representing the instantaneous AP frame-to-frame displacement of gut tissue as a function of the distance along the gut. Evaluating this over time, we generated a quantitative spatiotemporal map (QSTMap) of AP displacement as a function of AP position and time (Fig. 1C).

We also provide an example of a QSTMap calculated from DV displacements, again averaged along the DV axis (Fig. 2). Comparison of the AP and DV maps reveals, for example, a strong correlation between the two, as well as the phase shift between longitudinal (AP) and transverse (DV) displacements traveling along the gut (Fig. 2C). Notably, measures of perpendicular intestinal distortions have been performed in prior work, in which D-Maps deduced from intestinal diameters and L-Maps deduced from image correlations were obtained from gut sections [(20, 21, 32), see also references in (15)]. We demonstrate here that both of these projections can be inferred with a single technique from image correlation data. The isotropy of the correlation analysis enables direct comparison of the magnitudes of the intestinal motions along any axes. In the larval zebrafish examined, for example, DV displacements are weaker than AP displacements (Fig. 2A,B).

The QSTMap has similarities to STMaps used in previous studies [e.g. (11–14)]. The frequency of gut motility events can be inferred from their temporal spacing (Fig. 1B, green arrow, and 1D, green bracket), and the wave speed is given by the slope of linear features in the map (Fig. 1B, orange arrow, and 1D, orange arrow). The intensity of a QSTMap gives the instantaneous velocity of image elements, proportional to the amplitude of motility events, which we make use of below.

To more robustly quantify wave frequency and speed, we calculated the cross-correlation of the QSTMap: at each AP position (x) and time (t), we calculated the product of the QSTMap value and its value at a position and time shifted by (Δx, Δt), and then average over all x and t (Fig. 1D). A wavelike mode of velocity v, for example, will be well-correlated with an image of itself shifted by $\Delta x = v\,\Delta t$, while random motions will, on average, be uncorrelated. The time shift of the first local maximum at $\Delta x = 0$ represents the periodicity of gut motility (green bracket in Fig. 1D). The inverse slope of the peaks in the cross-correlation map

corresponds to the wave speed (orange arrow in Fig. 1D). Parameters such as the wave duration and the variance of wave speed could also be determined.

To characterize the amplitude of gut motility events, we applied spectral analysis to the QSTMap, highlighting periodic signals and quantifying their magnitude. We calculated the one-dimensional Fourier transform of the QSTMap displacement at each AP position (x), decomposing the time-varying function into contributions from each of the range of possible frequencies. The QSTMap has units of distance, as does its Fourier Transform. The square of the Fourier transform, known as the power spectral density, is composed of strong peaks at the frequencies of gut motility events (Fig. 1E), namely the primary frequency (red box) and its harmonics. We defined the gut motility amplitude as the average of the magnitude of the Fourier transform at the primary event frequency. This amplitude therefore also has units of distance, and can be thought of as the mean displacement per frame, for motions occurring at the event frequency. One could equivalently multiply this amplitude by the frame rate to refer to the velocity of the gut motions.

Acetylcholine increases the frequency and amplitude of gut motility in zebrafish larvae

The neurotransmitter acetylcholine (ACh) has been shown to increase the frequency of movements in the developing zebrafish gut at several different developmental stages (14, 29). To test our image analysis method in an experimental setting with an expected outcome, we treated 6 dpf wild-type larvae with 2.5 mg/ml ACh and compared their gut motility with that of untreated siblings. DICM videos were taken at 5 frames per second (fps) for 5 minute durations and analyzed as described above. A description of the relationship between frame rate, imaging duration, and frequency resolution is provided in the Methods. In agreement with Shi and colleagues (29), frequencies were generally higher for ACh-treated larvae than for controls (Fig. 3A), with mean ± s.e.m. values 2.38 ± 0.03 min^{-1} and 2.23 ± 0.05 min^{-1}, respectively. In particular, only a few ACh-treated larvae showed frequencies that were lower than the median of the frequencies for untreated, control larvae, and the standard deviation of the motility frequencies for ACh-treated larvae was also lower than for the control larvae (Fig. 3A). The ratio of the mean frequencies for treated (N=31) and untreated (N=30) larvae in our experiments is 1.07 ± 0.03, clearly greater than 1, as was also the case in the Shi et al. study in which frequency was assessed from manual counting of occurrences of folds in the gut (29).

To further examine the utility of our program, we extracted information about the wave propagation speed and amplitude of motility events. ACh-treated larvae exhibited no difference in wave speed compared to controls (Suppl. Fig. 1). However, 2.5 mg/ml ACh increased the median motility amplitude by over 50% (Fig. 3B). The mean ± s.e.m. amplitude values at 0.2 seconds per frame were 0.13 ± 0.02 μm and 0.10 ± 0.01 μm for ACh-treated and control larvae, respectively. Increased larval gut contraction strength has not been reported previously, but is reminiscent of similar ACh-induced effects seen in *ex vivo* smooth muscle preparations from adult zebrafish (14).

Feeding increases gut motility frequency and sustains amplitude during development

Food is well-known to influence gut motility, in particular by triggering contractile waves often referred to as peristaltic motions (4, 7). In zebrafish, the influence of food on gut motility patterns has not previously been assessed. We predicted that food-induced contractions would lead to observable and quantifiable increases in motility amplitude. To test this hypothesis, we compared gut motility parameters in both fed and unfed siblings over three days of development from 5-7 dpf. As before, 5 minute DICM videos were taken at 5 fps and analyzed. Videos in which food pieces were evident within the gut were discarded, as velocimetry is unable to distinguish cellular movement from food movement.

We compared gut motility frequency (Fig. 4A) and amplitude (Fig. 4B) in both fed and unfed siblings. Surprisingly, we found that feeding larvae alters the frequency of gut motility. At 5 dpf, there is little difference between fed and unfed larvae (Fig. 4A). However, for the next two days of integrated food consumption, fed gut motility frequency diverges away from that of unfed siblings (2.24 ± 0.03 min^{-1} and 2.06 ± 0.03 min^{-1} for 6 dpf fed and unfed, respectively, and 2.45 ± 0.06 min^{-1} and 2.10 ± 0.06 min^{-1} for 7 dpf). Strikingly, whereas unfed larvae appear to have monotonically decreasing frequency with age, fed larvae show higher gut motility frequency at 7 dpf than at 6 dpf (Fig. 4A).

As expected, zebrafish gut motility amplitude increased with feeding, though in an age-dependent manner (Fig. 4B). At 5 dpf, after one day of feeding, little change in amplitude is evident (Fig. 4B). However, for the next two days of integrated food consumption, the amplitude difference between fed and unfed larvae increases, with the median value in fed larvae being 1.4 times greater than in unfed larvae at 6 dpf, and 6.5 times greater at 7 dpf. The mean ± s.e.m. values were 0.14 ± 0.05 μm and 0.06 ± 0.01 μm for fed and unfed larvae respectively at 6 dpf, and 0.10 ± 0.02 μm and 0.03 ± 0.01 μm at 7 dpf. At both 6 and 7 dpf, feeding also leads to an increased spread in the amplitude data (Fig. 4B).

Larvae lacking ENS innervation display decreased motility amplitude

Changes in ENS innervation are known to affect gut motility (33–35). We analyzed gut motility parameters in 5-7 dpf *ret*$^{hu2846/hu2846}$ (hereafter referred to as *ret*$^{-/-}$) mutants. These fish lack ENS innervation and serve as models for Hirschsprung disease, a human congenital ENS disorder. Surprisingly, we found no discernible difference in frequency (Fig. 5A) or wave velocity (Suppl. Fig. 2), in contrast to a recent study reporting reductions in these parameters in 7 dpf *ret* mutant larvae (33). However, we found that on average, zebrafish *ret* mutants show reduced gut motility amplitudes compared to wild-type siblings at all days examined (Fig. 5B). We previously noted the lower motility amplitude of *ret* mutants, using an early version of this analysis approach (28).

Variability in gut motility parameters is dependent on the ENS

The amplitudes of gut motility events show considerable variability between individuals, especially among wild-type larvae (Fig. 5). We hypothesized that this variability would also be manifested within individuals over longer observation times, and that the ENS contributes to this variability, thus it would be larger in wild-types than in *ret* mutant larvae. To test this hypothesis, we imaged 6 dpf larvae for approximately 90 minutes, and analyzed the

resulting gut motility patterns as described above, generating spectral signatures of 4 minute sliding windows spanning the full duration of the movies (Fig. 6A,B). We found that wild-type larvae show a remarkable range of amplitudes over time both within and between individuals (Fig. 6A,C). In comparison, *ret* mutant larvae display much less amplitude variability within individuals (Fig. 6B,D).

Discussion

The complex motility patterns of the vertebrate gut are crucial to its function, and are modulated by developmental processes, physical and chemical stimuli, and the pathologies involved in a variety of disease states. The question of how to measure and characterize gut motility in a way that captures its essential features is therefore both important and timely.

Periodic, propagative contractions are critical for gut activity. For any periodic oscillatory motion, frequency and amplitude are essential and distinct characteristics. It has long been realized that data from imaging studies can readily yield gut motility frequencies and related properties such as wave propagation speeds, for example via image-derived STMaps. Straightforward yet robust amplitude measures have proven more challenging to obtain when imaging live animals. We therefore developed and assessed a new image analysis approach that combines image velocimetry, commonplace in studies of fluid dynamics, and spectral analysis, ubiquitous in signal processing applications, to provide quantitative measures of parameters related to both frequency and amplitude.

We apply this approach to data derived from DICM imaging of the larval zebrafish gut. DICM is well-suited to this analysis as it provides high contrast images of sub-cellular features as well as intrinsic optical sectioning. The former facilitates image velocimetry, as there are abundant features to correlate between video frames, while the latter avoids blurring and averaging over the depth of the sample. The data presented here were collected with a 40× objective lens and a field of view of approximately 400 μm. We suspect that 10× or 20× DICM optics would still provide adequate resolution for image correlation analysis, while providing a larger field of view.

We assessed our method in known as well as novel settings including ACh treatment, comparing fed to unfed zebrafish larvae, and analyzing zebrafish mutants lacking ENS innervation. Previous studies in zebrafish using conventional STMaps have found differences in parameters such as gut peristaltic frequency and the speed at which peristaltic waves travel along the gut for various phenotypes (33, 35, 36) and experimental conditions (14, 37, 38). We have shown, however, that there exist phenotypes that are identical in frequency or wave speed that are nonetheless different in the amplitude of gut motility, highlighting the importance of examining this axis of behavior. In addition, even for known experimental settings like treatment with ACh, we found that in addition to the expected increase in frequency, the amplitude of gut movements is also increased. Our program allows a more comprehensive analysis of gut motility parameters. Furthermore, the framework of cross-correlations, spectral analysis, and open-source software enables additional parameter extractions, if desired. The image analysis method presented here quantifies imaged motions in an automated and reproducible manner. In addition, it is

agnostic to the types of images it analyzes, making it versatile for a variety of cellular movements.

Due to the indiscriminate and automated nature of the analysis, a wider range of movements will be recorded when compared with methods that make use of manual feature identification. Consequently, some of the parameters defined in this study may not correspond directly to parameters obtained in previous research. As an example, previous studies have defined the frequency of gut motility only when a sustained wave travels along a large enough distance of the gut. In contrast, our method will identify the frequency of any periodic motion, whether it is a standard motility event or a single muscle cell firing repeatedly. In future applications, the user could define their own parameters from the QSTMap or from even the raw velocity vector field.

Our observation of increased gut motility frequency and amplitude in fed, compared to unfed, larval zebrafish provides the first assessment of how feeding alters motility in these animals. It is well-known in general that *s*pecific gut movements are triggered by food (7, 14). In mammals, the gut either displays stationary contractions that are non-propulsive and are necessary for mixing food or propulsive contractions that transport gut contents (8, 14). Our findings point to rich dynamics that can be rigorously studied in zebrafish, varying for example the duration and type of feeding. Food may also shape the microbial composition of the gut, as recent work has shown that apparent inter-microbial competition can be governed by gut motility(28) and that zebrafish mutants with altered motility assemble communities that can be distinguished by abundance of particular members (27). It should be noted that our imaging-based approach does not directly measure the forces applied by intestinal contractions. Experiments using, for example, ingested deformable particles of known stiffness may enable further insights into intestinal mechanics.

Our examination of gut motility parameters in *ret* mutant zebrafish larvae lacking ENS innervation highlights both the utility of our analysis and the complexity of mechanisms underlying gut motility. Heanue and colleagues (33) examined gut motility parameters in 7 dpf *ret* mutant larvae and found reduced frequency, contraction distance and contractile velocity of contractions along the whole length of the gut compared to wild-type siblings (33). In contrast, our study focusing on a segment of the mid-gut found a noticeable difference in amplitude but did not find differences in frequency or speed between 5 dpf and 7 dpf. The mutant allele used in these two studies is the same (ret^{hu2846}) and the mutant larvae show the same phenotype regarding enteric neurons, namely a total lack of neurons except for a few in the intestinal bulb [Suppl. Fig 3; (33)]. However, the two mutant lines have been maintained on different wild-type backgrounds [Tubingen Longfin, (33), AB (our study)]. Additionally, in contrast to the study of Heanue and colleagues (33), we do not observe an ENS phenotype with fewer neurons and altered gut motility in heterozygous larvae. One possible explanation for the difference in the gut motility defect is differences in the genetic background due to differences in the wild-type lines, most likely related to the high degree of heterogeneity in the number of SNPs between different genetic backgrounds in zebrafish (39). The high degree of genetic heterogeneity in zebrafish could also contribute to a higher degree of variability in gut motility parameters, which contributes to the advantages of using zebrafish as a disease model for studying gut motility parameters, as

human populations also display a high degree of genetic variation. In addition, this difference may also be due to evaluating gut motility in a segment of the gut with high resolution compared to evaluating only contractions that extend along the entire length of the gut. Interestingly, this difference is very reminiscent of Hirschsprung disease, a genetically complex disorder that displays significant phenotypic variation, for example differences in the extent of intestinal aganglionosis, even among individuals with the same mutant alleles (3). These results highlight the importance of detecting complementary and independent gut motility parameters, as in our *ret* mutants on the AB background only amplitude was affected. If we had analyzed our data using established methods, we would have concluded that gut motility parameters did not differ between in *ret* mutant larvae and their wild-type siblings. Thus, this newly developed approach provides additional parameters that may be differentially affected in different enteric neuropathies or gut diseases.

Phenotypic variation is a hallmark of ENS diseases such as Hirschsprung disease. We observe in general a noticeable degree of variability within and among individual zebrafish larvae with regard to gut motility amplitude (Fig. 6). This variability is displayed in all the data measurements, but becomes most apparent during longitudinal imaging. It has been previously reported that the speed of gut transit varies considerably among individuals (40). We suggest that the variability represents different gut motility modes that reflect different gut states at any given time point, for example the difference between when food is being mixed and when nutrients are being absorbed, which is then reflected in amplitude differences. Whereas two of the larvae shown in Fig. 6 show strong, varying increases in amplitude, the three other larvae show moderate changes in amplitude. In contrast, *ret* mutant larvae show very little change in amplitude over time. The ENS provides the intrinsic gut innervation that regulates gut movements (4). We propose that these amplitude changes are regulated by the ENS and may thus be absent from *ret* mutant larvae, motivating future work to establish connections between gut motility modes and specific ENS neuronal activity, and their alteration in the course of gut diseases.

Materials and Methods

Zebrafish Husbandry

All experiments were carried out in accordance with animal welfare laws, guidelines and policies and were approved by the University of Oregon Institutional Animal Care and Use Committee. Wild-type and ret^{hu2846} embryos were allowed to develop at 28.5°C and staged by hours post fertilization according to morphological criteria (41). Wild-types and ret^{hu2846} were of the AB background.

Imaging Experiments

Specimen mounting was performed as described previously (42). Briefly, larvae were anesthetized in 80 μg/ml tricaine methanesulfonate (Western Chemical, Ferndale, WA) for several minutes at 28.0 ± 0.2 °C. Larvae were then immersed in a liquified 0.5% agar gel (maximum temperature 42°C) and drawn into a glass capillary. The gel, once solidified, was mounted onto a microscope imaging chamber containing embryo medium (EM) with 80 μg/ml tricaine methanesulfonate maintained at 28°C. The solidified gel and the larva were

extruded into the imaging path to prevent the capillary glass from interfering with imaging. The mid-region of the gut was imaged, approximately 200 μm anterior of the anus (vent).

Imaging was performed using a custom-designed and custom-built microscope capable of differential interference contrast microscopy as well as light sheet fluorescence microscopy (23). The specimen was illuminated by a polarized 447nm LED (Quadica Developments Luxeon Star Brantford, Ontario, Canada) and imaged using a standard microscope objective (Zeiss Oberkochen, Germany DIC Plan Apochromat, 40×/1.0). A Nomarski prism and polarizer were oriented in such a way as to provide Differential Interference Contrast (DIC) (23). The resulting image was then focused onto a sCMOS Camera (Cooke, Kelheim, Germany, pco.edge). Movies were taken with 1 ms exposure times at 5 frames per second.

The imaging frame rate (here, f_{im} = 5 fps) sets the maximum frequency of gut motion that can be analyzed, $f_{max} = f_{im}/2$. (This is a general truth about time-series analysis; this maximum is known as the Nyquist frequency.) The Nyuquist frequency together with the overall duration of the movie set the frequency resolution, which is f_{max} divided by the number of time points analyzed. Collecting data at 5 frames per second for 5 minutes gives 1500 images per dataset, and therefore a frequency resolution of 0.1 oscillations per minute. Given the observed frequencies of gut motility events (2–3 oscillations per minute), a frequency resolution of 0.1 oscillations per minute enables high precision (<5%) characterization of motility.

Acetylcholine treatment

Wild-type larvae were raised in EM until 6 dpf. Acetylcholine treatments were essentially performed as previously described (29). Briefly, larvae were individually transferred to EM containing either 0.5% DMSO or 0.5% DMSO with Acetylcholine Chloride (Sigma-Aldrich, A6625; 2.5 mg/mL). Larvae were exposed to these conditions for a total of 20-30 minutes, anesthetized with tricaine for several minutes at 28°C, and mounted for imaging as described above.

Feeding of zebrafish larvae

Wild-type larvae were raised in EM until 4 dpf and transferred to embryo medium at 5 parts per thousand salinity (E5) in a new dish and rotifers were added to the dish. Fresh rotifers were added at 5 dpf and 6 dpf, so the fed zebrafish larvae had food *ad libidum*; 7 dpf fish were provided food for three days. Larvae were examined to ensure they had no food in their gut immediately prior to imaging, as PIV may track gut contents, such as food, instead of the gut wall.

Particle Image Velocimetry (PIV) and Quantitative Spatiotemporal Maps (QSTMaps)

PIV is a well-established image analysis technique that takes as its input a set of images and outputs a corresponding set of velocity vector fields representative of the motion contained within those images. To perform PIV, we used publicly available software called “PIVLab” [http://pivlab.blogspot.com] in addition to several home-built Matlab programs, provided as Supplementary Material.

A comprehensive description of how PIV works, its many different implementations, and how it is optimized can be found elsewhere (30). However, a simple example, representative of the key features of the technique, is as follows: A two-dimensional image $I_p(x,y)$ (known as an "interrogation area," possibly the subset of an even larger image) at frame p of an image series is subdivided into a grid. We denote the subset of $I_p(x,y)$ centered at grid element (i,j) as the template $t_{p,ij}(x,y)$. For each template in frame p, the cross correlation with the frame (p+1) is calculated:

$$C(x',y') = \sum_x \sum_y t_p(x,y) I_{p+1}(x-x', y-y')$$

The location of the maximum of $C(x',y')$ gives the most likely displacement of that template neighborhood from one frame to the next. The x' and y' at which C is maximum for each template correspond to each of the red arrows in Fig. 1B and Suppl. Movie 1. This is repeated over all grid elements to generate a displacement or velocity vector field, and then is repeated over all pairs of frames.

For this study, we used a first pass template size of 32 pixels corresponding to 20.8 microns in the image plane. Preliminary preprocessing consists of using PIVLab's built in PIVlab_preproc function, using contrast enhancement (CLAHE, size 50) and a high pass filter (size of 15 pixels). PIVLab then performs PIV over the entire image, segregating the resultant velocity vector field into a grid whose vertices are separated by 32 pixels. After this processing, a user defined mask is applied to the region of interest (in our case, an area containing the gut) and vertices outside of the mask are discarded.

As the geometry of the gut is not conserved in space or between individual larvae, masking results in the remaining vertex positions and numbers being spatially inconsistent from one data set to another and difficult to deal with numerically. To manage this, a new grid is generated to better accommodate the unique geometry. This new grid has a constant number of rows and columns and is distributed inside the mask in such a way as to fill most of the area. To do this, a curve is drawn by the user which represents the centerline of the mask (not necessarily the geometric center; in our case, the gut lumen). At each discrete position along the curve (equal in distance to the original PIV spacing), a constant number of vertices is distributed orthogonal to the curve at that position. This results in axes which, while spatially varying, are a better representation of the DV and AP axes of the gut (Suppl. Movie 1). The original velocity field is transformed to the new grid by bilinear interpolation and is its components are projected into the local DV and AP components.

We generate a QSTMap from the resulting velocity field. We are primarily concerned with the AP component of motion, and its variation along the AP axis. For nearly all the data presented, we therefore average the AP component of the frame-to-frame displacements along the DV direction, resulting in a one-dimensional map of displacement as a function of AP position, for each point in time (represented in the bottom half of Suppl. Movie 1). Plotting these functions over time gives the QSTMap. A representative data set is shown in

Figure 1C. Our software can assess DV displacements as well (Fig. 2), and equivalent analyses of transverse wave characteristics can be implemented by modifying the code.

Cross-Correlation Plots Define Frequency and Wave Speed

Larval gut motility waveforms can be individualized and complex. For most cases, the velocity waveform does not have a well-defined set of maxima that can clearly be followed across position and time. These waves, however, often have similar structures that repeat over time. Because of this, we take the QSTMap, $Q(x,t)$, and apply the cross correlation

$$C(dx,dt)=\sum_{x=0}^{L(dx)}\sum_{t=0}^{T(dt)}\left(\frac{1}{L(dx)T(dt)}\right)Q(x,t)Q(x-dx,t-dt)$$

where $L(dx) = L_0$ - dx is the length of the gut that can be examined for a given offset dx, L_0 is the total AP length of the analyzed gut segment (typically around 400 μm), $T(dt) = T_0$ - dt is the time that can be examined for a given offset dt, T_0 is the total time of the analyzed video (typically around 5 minutes).

An example of the resulting cross correlation is shown in Figure 1D. Even for multi-modal waveforms, the cross correlation results in a well-defined set of maxima that linearly increase over changes in distance. Therefore, we find the locations of the maximum of C and fit it to a line. The inverse slope of this line (Figure 1D, orange arrow) is defined as the wave speed.

The first non-zero peak in the autocorrelation of a signal is the time at which velocities at any position in the gut are most similar with themselves. The location of this peak therefore provides a robust measure of the frequency (Figure 1D, green bracket).

Spectral Analysis Defines Amplitude

To define amplitude, we needed a measure that is robust against noise and that focuses on the periodic peristaltic events and ignores occasional large vectors that result from motions such as larvae moving. We therefore perform a Fourier Transform of our QSTMap at each AP position, transforming each $Q_x(t)$ into a function of frequency, f, rather than time:

$$Q(f)=\sum_{t=1}^{N}Q_x(t)e^{-2\pi i\cdot(t-1)(f-1)/N}$$

To obtain the signal strength (“power”) at any frequency, we take the modulus (the signal multiplied by its complex conjugate) of $Q_x(f)$. Having previously found the frequency of gut motility from the cross correlation, we define the amplitude as the square root of the power at the frequency of gut motility. $Q_x(t)$ has units of distance, and so the amplitude similarly has units of distance, and is therefore a measure of actual gut displacement. For simplicity, our analysis considers only the average of these values over the entire gut in the field of

view. Figure 1E, shows the resultant power spectrum of the QSTMap from Figure 1C, with the red box outlining the peak power at the frequency of gut motility.

Supplementary Material

Refer to Web version on PubMed Central for supplementary material.

Acknowledgments

The authors thank Brandon Schlomann, Savannah Logan, Eric Corwin, and Karen Guillemin for useful discussions. Research reported in this publication was supported by the NIH as follows: NIGMS award P50GM098911 and NICHD award P01HD22486. The content is solely the responsibility of the authors and does not represent the official views of the NIH. Research reported in this publication was also supported by the National Science Foundation under award numbers 0922951 and 1427957, the M.J. Murdock Charitable Trust, and a REACHirschsprungs Foundation Research Grant (to JG).

References

1. Brosens E, Burns AJ, Brooks AS, et al. Genetics of enteric neuropathies. Dev Biol. 2016; 417:198–208. [PubMed: 27426273]
2. Goldstein AM, Nagy N. A bird's eye view of enteric nervous system development: lessons from the avian embryo. Pediatr Res. 2008; 64:326–333. [PubMed: 18636038]
3. Heanue TA, Pachnis V. Enteric nervous system development and Hirschsprung's disease: advances in genetic and stem cell studies. Nat Rev Neurosci. 2007; 8:466–479. [PubMed: 17514199]
4. Furness JB. The enteric nervous system. Oxford: Blackwell Publishing; 2006.
5. Huizinga JD, Lammers WJ. Gut peristalsis is governed by a multitude of cooperating mechanisms. Am J Physiol Gastrointest Liver Physiol. 2009; 296:G1–8. [PubMed: 18988693]
6. Deloose E, Janssen P, Depoortere I, Tack J. The migrating motor complex: control mechanisms and its role in health and disease. Nat Rev Gastroenterol Hepatol. 2012; 9:271–285. [PubMed: 22450306]
7. Olsson C, Holmgren S. Autonomic control of gut motility: a comparative view. Auton Neurosci. 2011; 165:80–101. [PubMed: 20724224]
8. Wood JD. Enteric nervous system: reflexes, pattern generators and motility. Curr Opin Gastroenterol. 2008; 24:149–158. [PubMed: 18301264]
9. Sanders KM, Ward SM, Koh SD. Interstitial cells: regulators of smooth muscle function. Physiol Rev. 2014; 94:859–907. [PubMed: 24987007]
10. Furness JB, Callaghan BP, Rivera LR, Cho HJ. The enteric nervous system and gastrointestinal innervation: integrated local and central control. Adv Exp Med Biol. 2014; 817:39–71. [PubMed: 24997029]
11. Hennig GW, Costa M, Chen BN, Brookes SJ. Quantitative analysis of peristalsis in the guinea-pig small intestine using spatio-temporal maps. J Physiol. 1999; 517(Pt 2):575–590. [PubMed: 10332103]
12. Janssen P, Lentle R. Spatiotemporal Mapping Techniques for Quantifying Gut Motility. In: Cheng LK, editorNew Advances in Gastrointestinal Motility Research. Springer Science; 2013.
13. Holmberg A, Schwerte T, Fritsche R, Pelster B, Holmgren S. Ontogeny of intestinal motility in correlation to neuronal development in zebrafish embryos and larvae. Journal of Fish Biology. 2003; 63:318–331.
14. Holmberg A, Schwerte T, Pelster B, Holmgren S. Ontogeny of the gut motility control system in zebrafish Danio rerio embryos and larvae. J Exp Biol. 2004; 207:4085–4094. [PubMed: 15498954]
15. Spencer NJ, Dinning PG, Brookes SJ, Costa M. Insights into the mechanisms underlying colonic motor patterns. J Physiol. 2016; 594:4099–4116. [PubMed: 26990133]
16. Bouchoucha M, Benard T, Dupres M. Temporal and spatial rhythmicity of jejunal wall motion in rats. Neurogastroenterol Motil. 1999; 11:339–346. [PubMed: 10520165]

17. Costa M, Wiklendt L, Arkwright JW, et al. An experimental method to identify neurogenic and myogenic active mechanical states of intestinal motility. Front Syst Neurosci. 2013; 7:7. [PubMed: 23596400]
18. Costa M, Wiklendt L, Simpson P, Spencer NJ, Brookes SJ, Dinning PG. Neuromechanical factors involved in the formation and propulsion of fecal pellets in the guinea-pig colon. Neurogastroenterol Motil. 2015; 27:1466–1477. [PubMed: 26251321]
19. Gwynne RM, Thomas EA, Goh SM, Sjovall H, Bornstein JC. Segmentation induced by intraluminal fatty acid in isolated guinea-pig duodenum and jejunum. J Physiol. 2004; 556:557–569. [PubMed: 14754993]
20. Lentle RG, Janssen PW, Asvarujanon P, Chambers P, Stafford KJ, Hemar Y. High-definition spatiotemporal mapping of contractile activity in the isolated proximal colon of the rabbit. J Comp Physiol B. 2008; 178:257–268. [PubMed: 17952441]
21. Lentle RG, Janssen PW, Asvarujanon P, Chambers P, Stafford KJ, Hemar Y. High definition mapping of circular and longitudinal motility in the terminal ileum of the brushtail possum Trichosurus vulpecula with watery and viscous perfusates. J Comp Physiol B. 2007; 177:543–556. [PubMed: 17342493]
22. Dinning PG, Arkwright JW, Costa M, et al. Temporal relationships between wall motion, intraluminal pressure, and flow in the isolated rabbit small intestine. Am J Physiol Gastrointest Liver Physiol. 2011; 300:G577–585. [PubMed: 21193528]
23. Baker RP, Taormina MJ, Jemielita M, Parthasarathy R. A combined light sheet fluorescence and differential interference contrast microscope for live imaging of multicellular specimens. J Microsc. 2015; 258:105–112. [PubMed: 25611324]
24. Ganz J, Melancon E, Eisen JS. Zebrafish as a model for understanding enteric nervous system interactions in the developing intestinal tract. Methods Cell Biol. 2016; 134:139–164. [PubMed: 27312493]
25. Ganz J. Gut feelings: Studying enteric nervous system development, function, and disease in the zebrafish model system. Dev Dyn. 2018; 247:268–278. [PubMed: 28975691]
26. Zhao X, Pack M. Modeling intestinal disorders using zebrafish. Methods Cell Biol. 2017; 138:241–270. [PubMed: 28129846]
27. Rolig AS, Mittge EK, Ganz J, et al. The enteric nervous system promotes intestinal health by constraining microbiota composition. PLoS Biol. 2017; 15:e2000689. [PubMed: 28207737]
28. Wiles TJ, Jemielita M, Baker RP, et al. Host Gut Motility Promotes Competitive Exclusion within a Model Intestinal Microbiota. PLoS Biol. 2016; 14:e1002517. [PubMed: 27458727]
29. Shi Y, Zhang Y, Zhao F, et al. Acetylcholine serves as a derepressor in Loperamide-induced Opioid-Induced Bowel Dysfunction (OIBD) in zebrafish. Sci Rep. 2014; 4:5602. [PubMed: 24998697]
30. Willert CE, Gharib M. Digital particle image velocimetry. Experiments in Fluids. 1991; 10:181–193.
31. Thielicke WS, E J. PIVlab – Towards User-friendly, Affordable and Accurate Digital Particle Image Velocimetry in MATLAB. Journal of Open Research Software. 2014; 2
32. Costa M, Dodds KN, Wiklendt L, Spencer NJ, Brookes SJ, Dinning PG. Neurogenic and myogenic motor activity in the colon of the guinea pig, mouse, rabbit, and rat. Am J Physiol Gastrointest Liver Physiol. 2013; 305:G749–759. [PubMed: 24052530]
33. Heanue TA, Boesmans W, Bell DM, Kawakami K, Vanden Berghe P, Pachnis V. A Novel Zebrafish ret Heterozygous Model of Hirschsprung Disease Identifies a Functional Role for mapk10 as a Modifier of Enteric Nervous System Phenotype Severity. PLoS Genet. 2016; 12:e1006439. [PubMed: 27902697]
34. Kuhlman J, Eisen JS. Genetic screen for mutations affecting development and function of the enteric nervous system. Dev Dyn. 2007; 236:118–127. [PubMed: 17131406]
35. Uyttebroek L, Shepherd IT, Vanden Berghe P, Hubens G, Timmermans JP, Van Nassauw L. The zebrafish mutant lessen: an experimental model for congenital enteric neuropathies. Neurogastroenterol Motil. 2016; 28:345–357. [PubMed: 26685876]

36. Rich A, Gordon S, Brown C, et al. Kit signaling is required for development of coordinated motility patterns in zebrafish gastrointestinal tract. Zebrafish. 2013; 10:154–160. [PubMed: 23297728]

37. Holmberg A, Olsson C, Hennig GW. TTX-sensitive and TTX-insensitive control of spontaneous gut motility in the developing zebrafish (Danio rerio) larvae. J Exp Biol. 2007; 210:1084–1091. [PubMed: 17337720]

38. Holmberg A, Olsson C, Holmgren S. The effects of endogenous and exogenous nitric oxide on gut motility in zebrafish Danio rerio embryos and larvae. J Exp Biol. 2006; 209:2472–2479. [PubMed: 16788030]

39. LaFave MC, Varshney GK, Vemulapalli M, Mullikin JC, Burgess SM. A defined zebrafish line for high-throughput genetics and genomics: NHGRI-1. Genetics. 2014; 198:167–170. [PubMed: 25009150]

40. Field HA, Kelley KA, Martell L, Goldstein AM, Serluca FC. Analysis of gastrointestinal physiology using a novel intestinal transit assay in zebrafish. Neurogastroenterol Motil. 2009; 21:304–312. [PubMed: 19140958]

41. Kimmel CB, Ballard WW, Kimmel SR, Ullmann B, Schilling TF. Stages of embryonic development of the zebrafish. Dev Dyn. 1995; 203:253–310. [PubMed: 8589427]

42. Jemielita M, Taormina MJ, Burns AR, et al. Spatial and temporal features of the growth of a bacterial species colonizing the zebrafish gut. MBio. 2014; 5

Key points

- Gut motility entails rhythmic, coordinated movements that are affected in many diseases. Existing approaches to the analysis of *in vivo* imaging data reveal properties related to the temporal frequency of motility patterns, but measures of spatial displacements have been elusive.
- We present an analysis technique using image velocimetry and spectral analysis that returns quantitative measures of gut contraction strength, frequency, and wave speed.
- This approach enables insights into gut dynamics in a variety of developmental and physiological contexts, including responses to chemical stimuli and genetic variation.

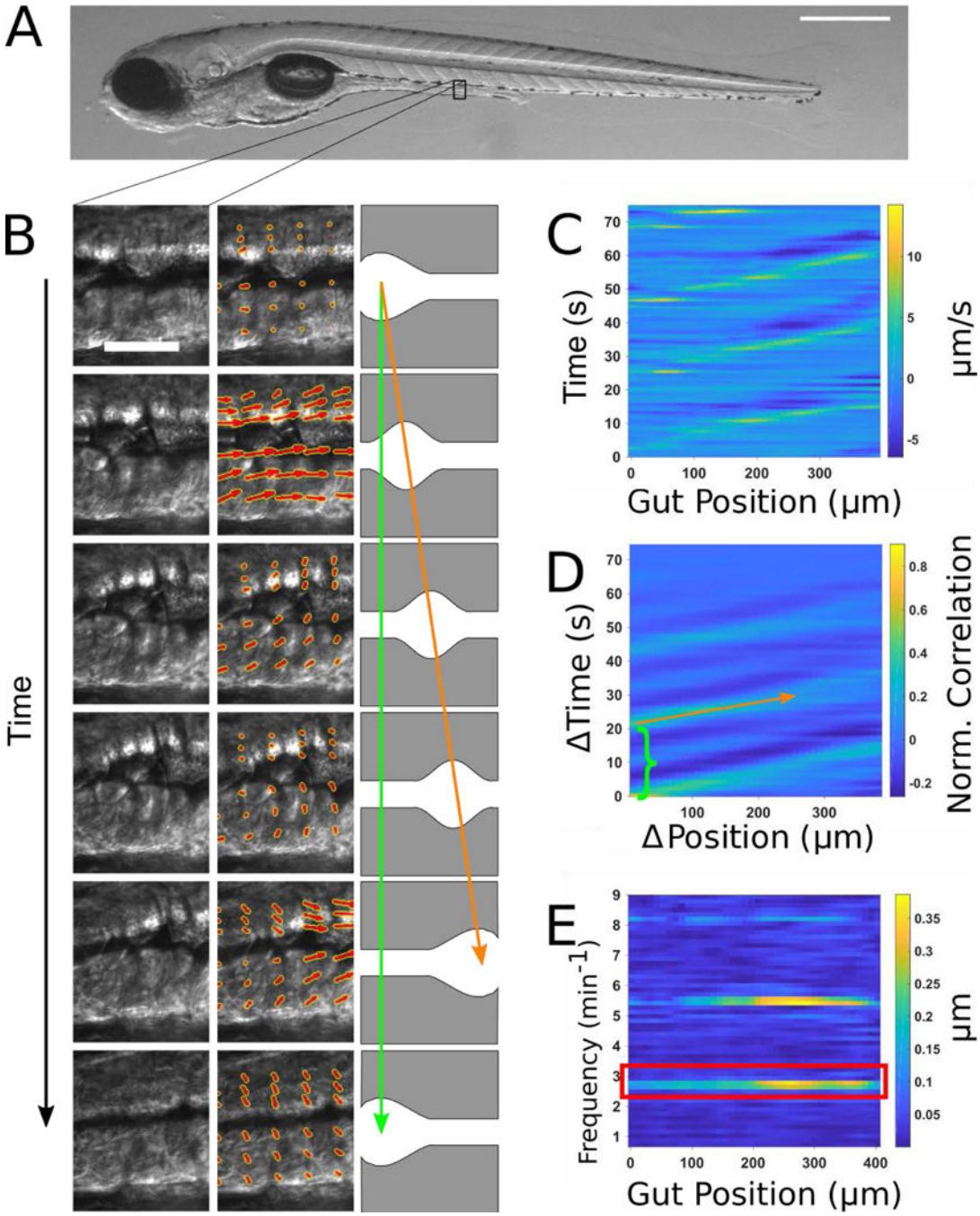

Figure 1. Illustration of gut motility analysis

(A) Brightfield image of a 6 dpf zebrafish larva. Scale bar: 500μm. (B) Left column: a representative series of DIC images of a small region of the midgut. Scale bar 25 μm. Center column: the velocity vector field (red arrows) obtained by performing Particle Image Velocimetry (PIV) on the image series. Right column: schematic illustration of coordinated movements from left to right (anterior to posterior). Wave speed is indicated by the slope of the orange arrow and periodicity indicated by the extent of the green arrow. (C) Quantitative Spatiotemporal Maps (QSTMaps) are obtained by averaging the anterior-posterior

component of the velocity vector field along the dorsal-ventral direction and then plotting the curve over time. The color axis represents the velocities, with positive and negative values denoting posterior and anterior movement, respectively. (D) An averaged cross correlation of the QSTMap more clearly reveals motility parameters. The period of motility events corresponds to the time of the first local maximum at ΔPosition = 0 autocorrelation (green bracket; analogous to the length of the green arrow in Fig. 1B). The wave speed corresponds to the inverse slope of maxima in the plot (orange arrow; analogous to the orange arrow in Fig. 1B). (E) A power spectrum of the QSTMap shows the magnitude of gut motion at various frequencies. The amplitude of motility events is determined from the average of the power spectrum at the motility frequency (red box).

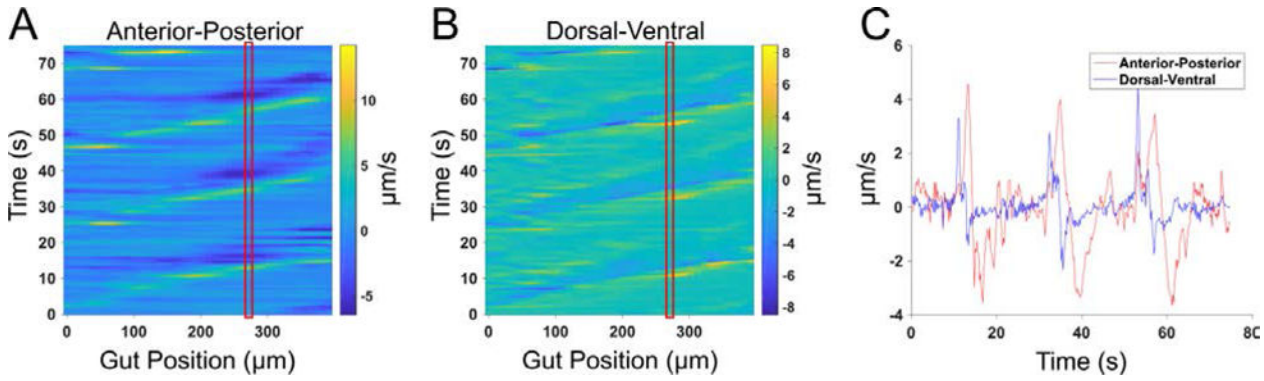

Figure 2.

Anterior-posterior (AP) and dorsal-ventral (DV) motility maps. (A) As in Figure 1C, QSTMap of the averaged AP component of the velocity vector field as a function of the distance down the gut. The color axis represents the velocities, with positive and negative values denoting posterior and anterior movement, respectively. (B) QSTMap of the averaged DV component of the velocity vector field as a function of the distance down the gut, from the same image data as (A). The color axis represents the velocities, with positive and negative values denoting outward and inward movement relative to the intestinal midline, respectively. (C) Gut motility velocities as a function of time at a fixed position along the gut, indicated by the red boxes in A and B, for both the AP and DV components of the averaged vector field. Both longitudinal and transverse motions are correlated, with the DV component lagging the AP component by a few seconds.

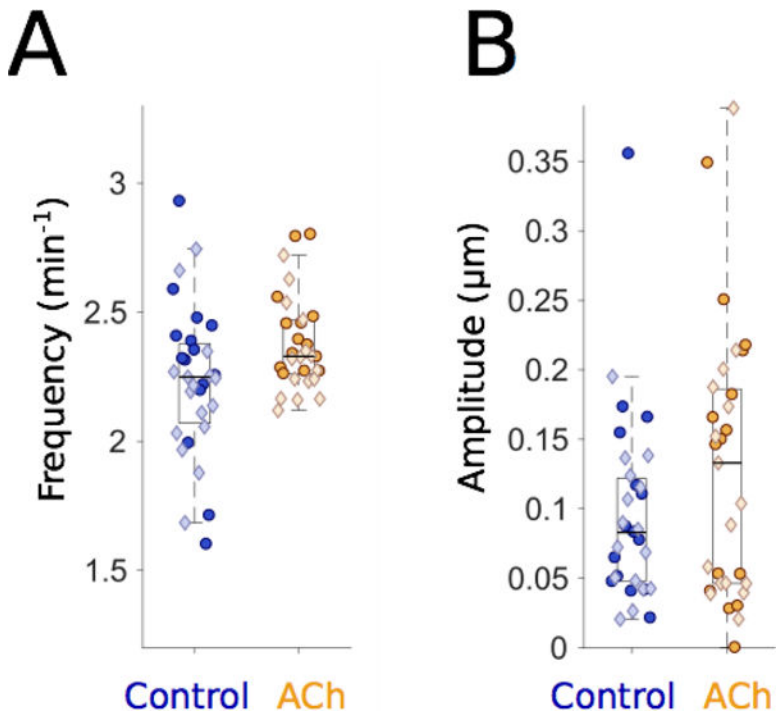

Figure 3. Acetylcholine alters the amplitude and frequency of gut motility

(A) Gut motility frequencies for 6 dpf control larvae (blue, n=31) and larvae immersed in 2.5 mg/ml acetylcholine (ACh; orange, n=30), showing an increased frequency in ACh-treated larvae (mean ± s.e.m. = 2.38 ± 0.03 min^{-1}) compared to untreated controls (2.23 ± 0.05 min^{-1}). Each point represents data from a five-minute video of a single larva, captured at five frames per second. Darker circles and lighter diamonds represent two independent experiments. (B) Gut motility amplitudes corresponding to the same experiments depicted in panel (A). Both the mean and the standard error of the mean of gut motility amplitudes for ACh-treated larvae (0.13 ± 0.02µm) are higher than controls (0.10 ± 0.01 µm).

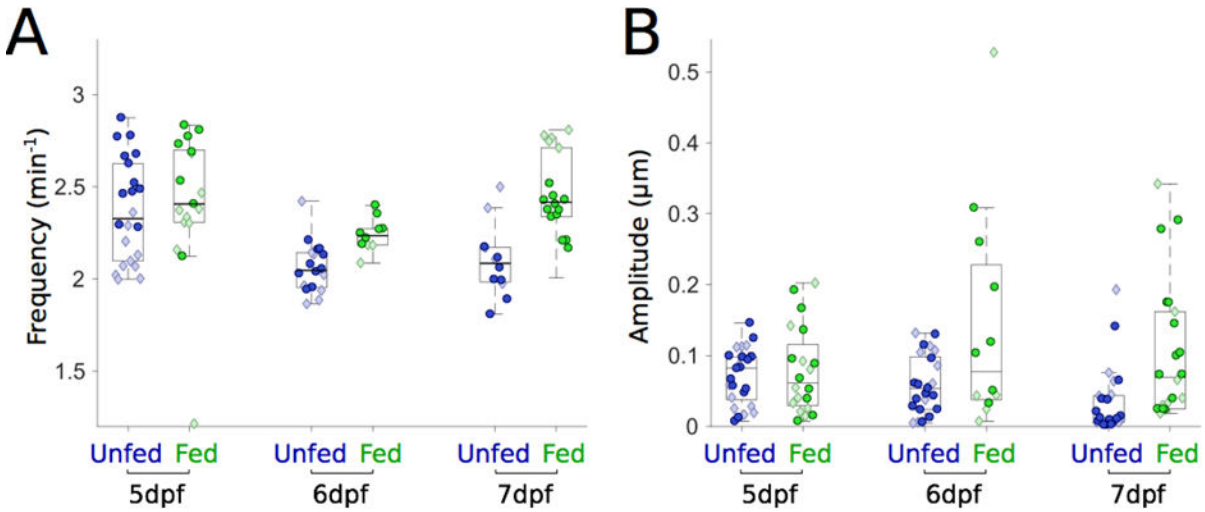

Figure 4. Feeding increases the frequency and amplitude of gut motility

(A) Gut motility frequencies for unfed (blue, n=22,18,12) and fed (green, n=17,10,18) larvae over three days of development. Frequencies of fed and unfed larvae remain similar after one day of feeding. Frequencies become different over the next two days, with fed larvae showing higher frequencies. Darker circles and lighter diamonds represent two independent experiments. (B) Gut motility amplitudes corresponding to the same experiments depicted in panel (A) for unfed (blue, n=25, 25, 25) and fed (green, n=20,12, 22). As in panel (A), amplitudes are similar to one another one day after feeding but the means become significantly different over the next two days.

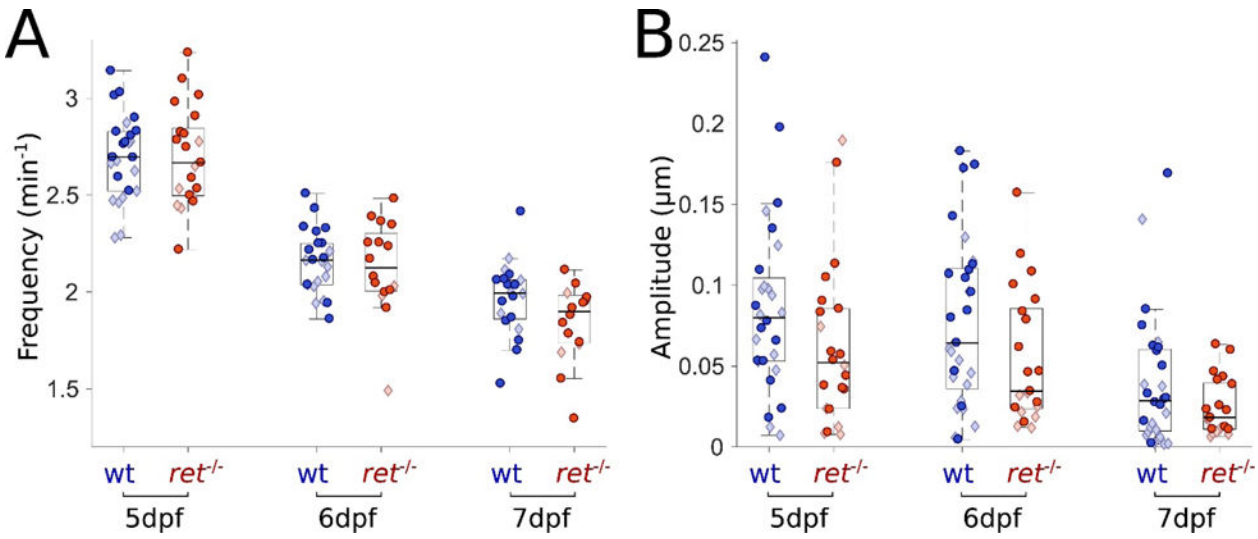

Figure 5. *ret* mutants lacking an ENS display similar frequencies and reduced amplitudes compared to wild-type siblings

(A) Gut motility frequencies for wild-type (wt) (blue, n=25, 23, 20) and *ret*$^{-/-}$ (red, n=21,16,16) larvae over three days of development. Frequencies of *ret*$^{-/-}$ and wt siblings are the same over three days of development. Darker circles and lighter diamonds represent two independent experiments. (B) Gut motility amplitudes corresponding to the same experiments depicted in panel (A) for wt (blue, n=28, 29, 28) and *ret*$^{-/-}$ (red, n=22, 21, 21). Amplitudes and standard deviations of those amplitudes of *ret* mutants are consistently lower over all three days compared to wt.

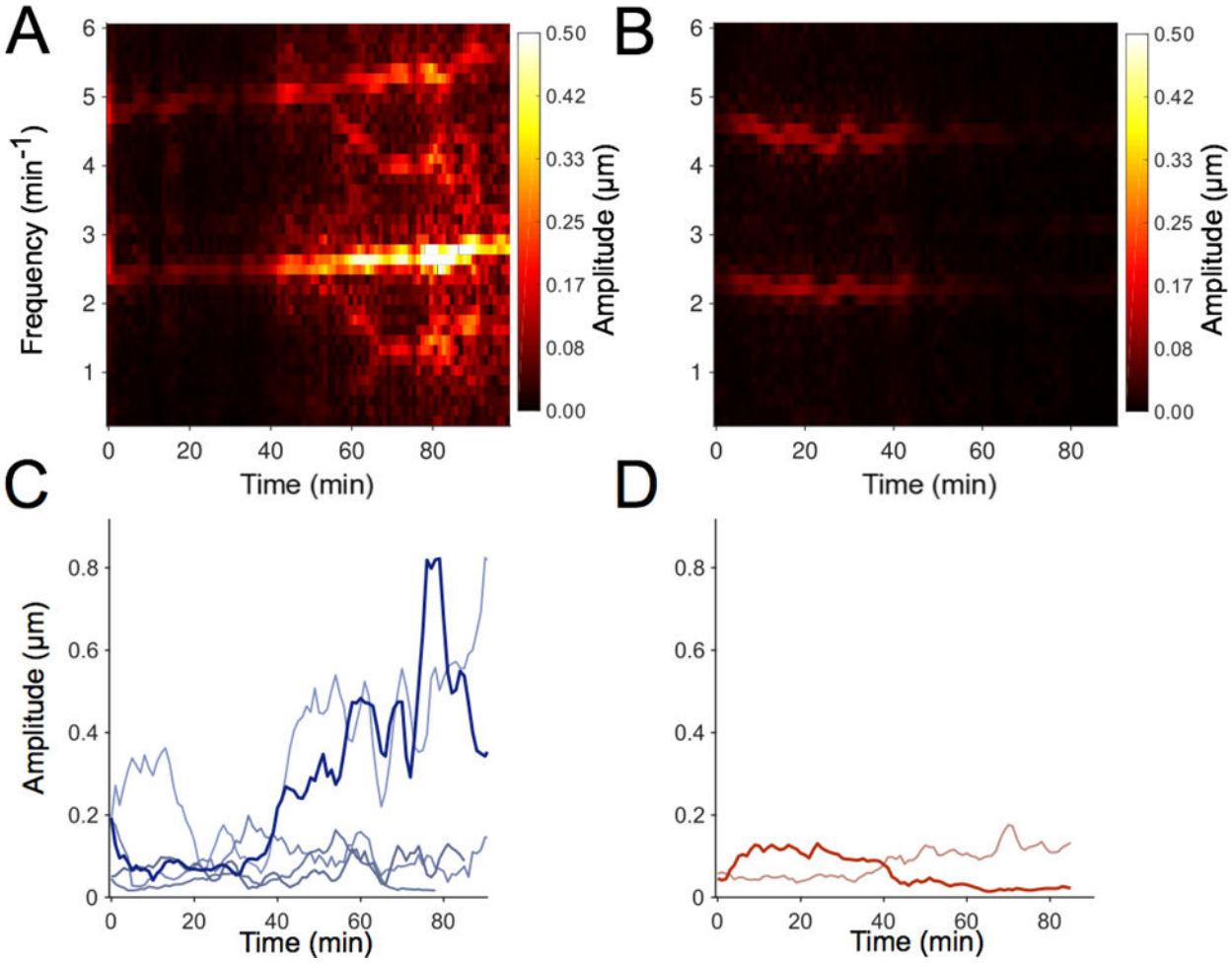

Figure 6. Wild-type larvae have higher amplitude variability than *ret* mutants

(A) Spectrogram illustrating the time-varying gut motility power spectrum of a wild-type (wt) larva over 1.5 hours. Each column depicts the power spectrum calculated over a 4-minute window. (B) A spectrogram of a single *ret* mutant larva. (C) Maximum Intensity Projections (MIP) of spectrograms for wt larvae (n=5); each curve represents a different larva. The bolded blue curve is the MIP of the spectrogram provided in (A). (D) MIP of the spectrograms for *ret* mutant larvae (n=2). The bolded red curve is the MIP of the spectrogram provided in (B). The amplitudes for both *ret* mutant larvae are lower and less variable over time than most wt larvae.